LAWRENCE
LIVERMORE
NATIONAL
LABORATORY

LLNL-PROC-400977

Performance of a MEMS-base Adaptive Optics Optical Coherency Tomography System

Julia Evans, Robert J. Zadwadzki, Steve Jones, Scot Olivier, Samelia Opkpodu, John S. Werner

February 4, 2008

Photonics West: MOEMS-MEMS 2008
San Jose, CA, United States
January 19, 2008 through January 24, 2008

Disclaimer

Extreme Adaptive Optics Testbed: Performance and Characterization of a 1024-MEMS Deformable Mirror

Julia W. Evans[a,b], Katie Morzinski[c], Scott Severson[c], Lisa Poyneer[a], Bruce Macintosh[a,c], Daren Dillon[c],Layra Reza[c,d], Donald Gavel[c], David Palmer[a], Scot Olivier[a], Paul Bierden[e]

[a]Lawrence Livermore National Laboratory, 7000 East Avenue, Livermore,USA
[b]University of California at Davis, One Shields Avenue, Davis, USA
[c]University of California at Santa Cruz, 1156 High Street, Santa Cruz, USA
[d]University of Texas at El Paso, 500 West University Avenue — El Paso, USA
[e]Boston Micromachines Corporation, 108 Water Street, Suite 2L Watertown, USA

ABSTRACT

We have demonstrated that a microelectrical mechanical systems (MEMS) deformable mirror can be flattened to < 1 nm RMS within controllable spatial frequencies over a 9.2-mm aperture making it a viable option for high-contrast adaptive optics systems (also known as Extreme Adaptive Optics). The Extreme Adaptive Optics Testbed at UC Santa Cruz is being used to investigate and develop technologies for high-contrast imaging, especially wavefront control. A phase shifting diffraction interferometer (PSDI) measures wavefront errors with sub-nm precision and accuracy for metrology and wavefront control. Consistent flattening, required testing and characterization of the individual actuator response, including the effects of dead and low-response actuators. Stability and repeatability of the MEMS devices was also tested. An error budget for MEMS closed loop performance will summarize MEMS characterization.

Keywords: Adaptive Optics, MEMS, Extreme Adaptive Optics

1. INTRODUCTION

High contrast adaptive optics, known as Extreme Adaptive Optics (ExAO), needed for extrasolar planet imaging has more stringent deformable mirror requirements than traditional adaptive optics.[1] The ExAO testbed in the Laboratory for Adaptive Optics (LAO) at UC Santa Cruz is investigating and developing technology including MEMS deformable mirrors (DMs) for an extrasolar planet imager. Current work includes performance testing and characterization of a 1024-MEMS device developed by Boston Micromachines Corporation (BMC).[2] We have flattened the DM to 0.54 nm RMS in the control band, exceeding our goal of 1 nm RMS. We also investigated stroke, unpowered shape, stability, and actuator uniformity.

2. EXPERIMENTAL METHOD

The ExAO testbed was designed with high-quality optics to ensure end-to-end wavefront error would be small (< 1.5 nm RMS). Initial high-contrast measurements focused on characterizing measurement techniques and instrumentation without the DM; in particular suppressing diffraction, understanding the high-contrast regime and developing experimental methods for high-contrast imaging (i.e. controlling scattered light).[3] In the current set-up a 1024-actuator MEMS deformable mirror, developed by BMC, is used for wavefront control. The testbed has two modes of operation: far-field imaging, and wavefront measurement interferometry. The testbed consists of a laser source (532 nm) passed through an optical fiber and a high quality (< 1 nm RMS) lens. The beam passes through a pupil stop and reflects off the flat or deformable mirror (DM). In imaging mode, the beam is then imaged onto a CCD sampled at ~ 5 times the Nyquist limit. (See Fig. 1). High-contrast measurements can be made directly in imaging mode when diffraction is suppressed with a prolate spheroid shaped pupil.[4] Preliminary contrast measurements with a flattened MEMS DM have been made.[5]

In Phase Shifting Diffraction Interferometer (PSDI) mode, the testbed becomes an extremely accurate ($<$ 0.5 nm RMS absolute wavefront accuracy) optical metrology system. The PSDI was developed at Lawrence Livermore National Laboratory for metrology of aspheric optics for UV wavelengths.[6] Briefly, a probe wavefront

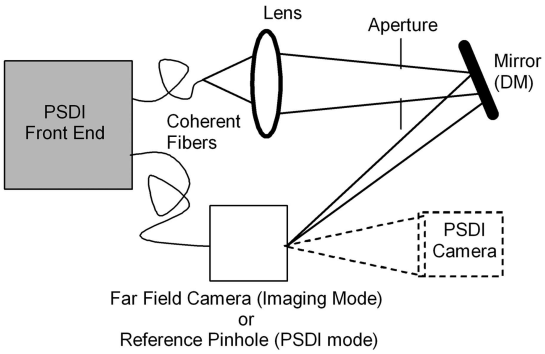

Figure 1. Simplified schematic of the ExAO testbed. The Testbed has two modes of operation: Imaging and PSDI. In PSDI mode the interferometer is used for metrology and wavefront control. Far field images can be captured in imaging mode.

is injected from the upper single-mode fiber in Fig. 1. This passes through the system and is focused onto a pinhole embedded in a super polished flat mirror (the reference pinhole). Meanwhile, a coherent reference beam passes through the pinhole and interferes with the outgoing probe wavefront. The interference pattern is recorded at a CCD located in an arbitrary location along the optical axis. Using standard phase-shifting interferometer techniques this produces a measurement of the fringe pattern at this location, which can then be converted to a wavefront and then numerically propagated to the plane of interest, such as the MEMS plane of the system. Wavefront measurements are used to control the MEMS during closed loop operations. The spatial resolution at the MEMS plane is limited by truncation effects due to an aperture at the reference pinhole. The effective resolution in the MEMS plane is ~ 141 microns.

For closed loop operation, programs in IDL are used to direct data acquisition, back propagation calculations and commands to the MEMS device through the MEMS driver. Before closed loop operation, the alignment and voltage response of the system must be calibrated. The voltage response of each actuator is measured and used during closed loop operations. The MEMS is controlled with 13-bit D/A conversion and amplification using a system developed by Red Nun Electronics Company. The smallest voltage step allowed with these electronics is 0.025 volts for the current set up.

3. MEMS CHARACTERIZATION

A series of 10 deformable mirrors delivered by BMC^2 have been tested in the Laboratory for Adaptive Optics (LAO). The lab environment is maintained at below 50% relative humidity to avoid damage to the devices.[7] The 340-micron actuators are run by 13-bit electronics at a maximum of 160 volts. We have not seen evidence of any damage occurring due to snap-down on any of the 10 devices. Unpowered, the best device has ~ 50 nm RMS wavefront error, an improvement over earlier devices that had over 200 nm RMS wavefront error. The closed loop results presented here were taken with the newest device, which has ~ 150 nm RMS unpowered wavefront error. Tests were done to measure the stroke and stability of the devices. Irregular actuators were also identified and characterized.

A Zygo interferometer with finer individual actuator sampling compared to the PSDI was used to measure the stroke of 4 DMs with no bias voltage applied. When a 3x3 array of adjacent actuators was moved the average stroke was 1221 nm; when an individual actuator was tested the average stroke was 836 nm. In practice the device is operated at a bias (usually 110 volts) reducing available deflection of individual actuators with respect to their neighbors. Current operations have a conservative voltage limit, but based on the displacement measurements a higher voltage limit (and increased stroke) might be possible without increased snap-down.

To test MEMS stability a flattened shape is applied to the MEMS device and successive wavefront measurements are taken every 38 seconds (the minimum time to complete a PSDI measurement) for 60 iterations. Short term stability is measured over 9 minute intervals within the long term stability test. The shorter time scale is comparable to typical closed loop operation times. The variation of each actuator in phase from its initial

position is calculated with piston and tip/tilt removed. This analysis was done over approximately one third of the device (367 actuators). Previous tests had indicated less stability[5] because of errors produced by the MEMS drive electronics that have since been corrected. The average long term stability of the MEMS was measured as 0.16 nm RMS phase. The system stability was measured to be 0.08 nm RMS by replacing the MEMS with a flat mirror. On the shorter time scale the MEMS is more stable with an average RMS deviation of 0.13 nm phase, while the system stability remained the same.

MEMS actuators have a non-linear response that varies some on a individual device and more between devices. We have the capability to calibrate the voltage response of every actuator on a device.This calibration also provides information on actuator uniformity. A few actuators have a particularly irregular response which could be an issue for closed loop high-contrast operation. The voltage response of several actuators on the

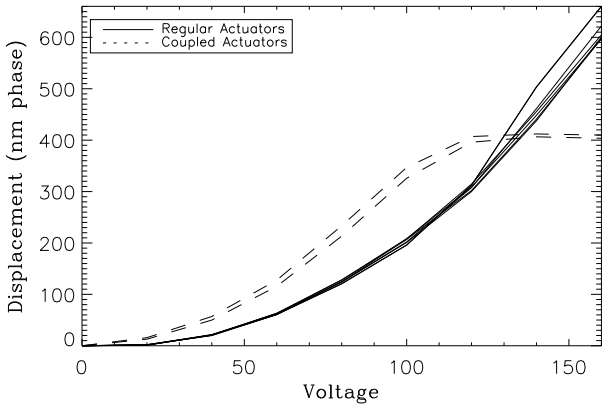

Figure 2. Voltage versus displacement (in nm phase) for select actuators on the best MEMS deformable mirror. The two irregular actuators are the only two in the aperture for this device and our coupled. The regular actuators have a variation of 2.6%

current (and also the device with the lowest RMS flattening) MEMS device are shown in Fig.2. This particular device has only two irregular actuators in the aperture. They are coupled (they move together) and both have no displacement beyond the bias voltage (See Fig.2). Excluding these two and actuators on the outer four rows/columns, the average maximum single actuator displacement (with a bias of 110 volts and applied voltage of 160 volts) is 629.5 nm phase, with a variation between actuators of 2.6%. The operational stroke during closed loop would actually be higher because actuators are not significantly displaced from their neighbors. From these tests we have categorized irregular actuators as no response, low response, coupled, and high response. No response actuators, or dead actuators, do not move with voltage applied or with their neighbors. Dead actuators in the aperture severely limit closed loop performance and must be avoided especially in high-contrast imaging applications. Low response actuators can be actuators that only move with their neighbors or actuators with odd voltage response curves like the coupled actuators on this device that do not move beyond the bias voltage. On the right in Fig.3 is the maximum voltage displacement for each actuator on a previous device. The center dark actuator is a low response actuator that only moves with its neighbors. After flattening, this actuator is offset from its neighbors by about 20 nm and thus limited closed loop performance of this device to 0.68 nm inside the band of spatial frequencies controllable by the DM. In previous tests with this device,[5] more irregular actuators were apparent due to errors in the driver electronics, but this electronics problem has since been corrected. The current device has many irregular actuators around the edge. Most of these are coupled or low response, but do not seem to significantly affect performance because of their position outside the aperture. High-response actuators have not been a problem in closed loop operation. In the course of testing the 10 devices we have seen a marked improvement in both yield and actuator uniformity. Early devices required smaller apertures during closed loop operation to avoid dead actuators. Note that the regular structure in both maximum displacement measurements is caused by a systematic measurement error.

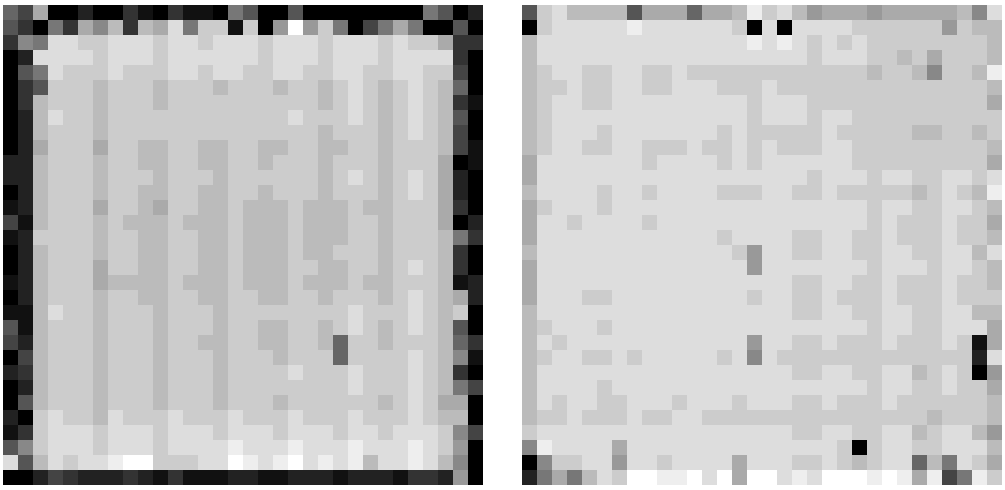

Figure 3. The maximum displacement for each actuator on the current device (left) and a previous device (right). The current device has no dead actuators outside of the outer edge actuators and only the two coupled irregular actuators inside the aperture. The older device had more dead actuators and several other irregular actuators which limited closed loop performance. Note that these are plotted on different scales as the older device had more stroke at 160 volts than the current device.

4. CLOSED LOOP PERFORMANCE

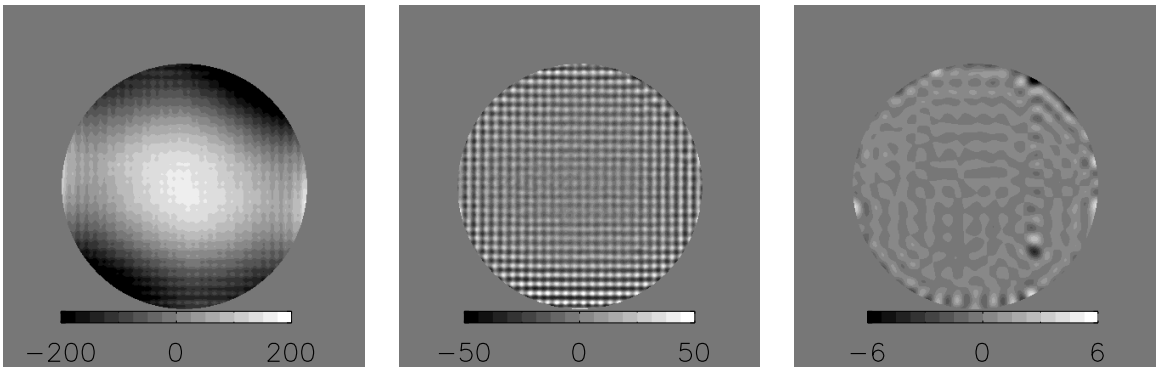

Figure 4. Wavefronts taken before and after a closed loop test. The initial wavefront has an RMS WFE of 148 nm, while the flattened wavefront has 12.8 nm total RMS wavefront error, which is mostly errors on the scale on an individual actuator. Only 0.54 nm is inside the controlled range of spatial frequencies. This is seen more clearly in the lowpass filtered image (far right).

In previous closed loop tests a 10-mm circular aperture was placed slightly in front of the MEMS device during flattening. In the most recent tests the physical aperture was removed and effectively replaced with a software aperture of the same size (9.2 mm in the MEMS plane) to reduce edge effects. A ring two actuators wide around the edge of the aperture is slaved to the final ring of actuators inside the aperture using a nearest neighbor average to further reduce edge effects. Typically the closed loop is run for between 12-15 iterations, and most of the correction takes place within the first five iterations. The test shown in Fig.4 was run for 25 iterations with the best flattening occurring at iteration 20. Tip/Tilt is not actively controlled; it is removed by hand after several iterations and numerically thereafter. Before running closed loop the wavefront had 148.1 nm total RMS wavefront error, and after flattening the wavefront had 12.8 nm total RMS wavefront error with 0.54 nm inside the controlled range of spatial frequencies. This device has more out-of-band wavefront error than previous devices, possibly because of a window attached to protect the device from humidity. The wavefront

improvement is noticeable in Fig. 4. The large structure of the errors in the initial wavefront have been corrected in the final wavefront (middle image), revealing smaller structures on the scale of an individual actuator. Those small-structure errors fall outside of the region of controllable errors. By filtering out those high-spatial-frequency errors the limitations to closed loop performance can be better investigated (far right image). The light and dark actuators slightly to the right and below center are the coupled actuators discussed previously. They are about 3 nm above and below their neighbors. The effective aperture has a 9.2 mm diameter with approximately 27 actuators across yielding a highest controllable spatial frequency of about 13.5 cycles per aperture and a corresponding control radius in the point spread function of $13.5\lambda/D$. The cutoff frequency is apparent in the

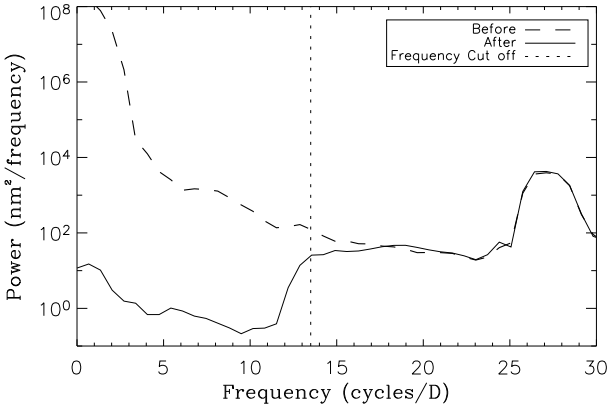

Figure 5. Power spectrum generated from wavefronts taken before and after closed loop routine.There were 27 actuators across the aperture yielding a highest controllable spatial frequency of 13.5 cycles per aperture. The bump at 27 cycles per aperture corresponds to physical structures on the MEMS at scale of the individual actuator spacing.

power spectrum (See Fig. 5) at the edge of the dark hole region. A bump in the power spectrum at 27 cycles per aperture indicates the error introduced by print through of physical structures on the MEMS device at the scale of an individual actuator.

5. LIMITATIONS TO IMPROVED PERFORMANCE

We have identified 5 error sources that limit closed loop performance and they are summarized in Table 1. The edge effect is measured by comparing the RMS WFE over the full aperture and over a 75% aperture. In previous results this error source was > 1 nm due to the distance between the physical aperture and the MEMS device. The physical aperture has been replaced with a software aperture and the edge effect has been reduced to 0.42 nm. Even with this reduction edge effects remain the largest error source and should be further investigated. The effect of irregular actuators on closed loop performance is clear from the lowpass filtered image (far right of Fig.4). Devices with more irregular actuators did not flatten as well as this device. The effect of the coupled actuators on flattening was estimated by comparing the RMS WFE over 75% of the aperture to the error over the same aperture with the area around the irregular actuators removed. This doesn't account for any errors caused by the irregular actuators outside of their immediate vicinity. The voltage step size is determined by the number of bits in the electronics split over the voltage range of the electronics, currently 0 to 200 volts. This error could be reduced with higher resolution drivers, or a change in the voltage range. The stability of the device was discussed previously. Measurement error is inherent to the PSDI system and is calculated by comparing two measurements taken consecutively in the converged system. Alignment errors of the input fiber of the PSDI measurement leg increase measurement error. The calculated wavefront error agrees well with the measured wavefront error indicating that these errors are the limiting errors for improved performance.

Error Source	nm RMS
Edge Effects	0.42
Irregular Actuators	0.22
Voltage Step Size	0.18
Stability	0.13
Measurement Error	0.20
Total	0.56

Table 1. Error budget for best flattening result.

6. CONCLUSIONS

Our testing has demonstrated that MEMS deformable mirrors are now feasible for astronomical adaptive optics systems, in particular for Extreme Adaptive Optics systems. MEMS DMs can be flattened to 0.54 nm RMS over controllable spatial frequencies. We have characterized stability and actuator uniformity and determined error sources which limit closed loop performance in an adaptive optics system. Improvements in yield and actuator uniformity have improved performance and the feasibility of these devices. Far-field contrast measurements with the improved flattening of the MEMS are in progress. Closed loop tests with the additional phase aberrations introduced to the system are also ongoing.

ACKNOWLEDGMENTS

Contact Julia Evans at `evans74@llnl.gov`.This work has been supported in part by the National Science Foundation Science and Technology Center for Adaptive Optics, managed by the University of California at Santa Cruz under cooperative agreement No. AST-9876783 and in part by the Gordon and Betty Moore Foundation through its grant to the UCO/Lick Laboratory for Adaptive Optics.This work was performed under the auspices of the U.S. Department of Energy by the University of California, Lawrence Livermore National Laboratory under contract No. W-7405-Eng-48.

REFERENCES

1. B. A. Macintosh, S. S. Olivier, B. J. Bauman, J. M. Brase, E. Carr, C. J. Carrano, D. T. Gavel, C. E. Max, and J. Patience, "Practical high-order adaptive optics systems for extrasolar planet searches," in *Adaptive Optics Systems and Technology II*, R. K. Tyson, D. Bonaccini, and M. C. Roggemann, eds., *Proc. SPIE* **4494**, pp. 60–68, 2002.
2. T. Bifano, P. Bierden, and J. Perreault, "Micromachined deformable mirrors for dynamic wavefront control," in *Advanced Wavefront Control:Methods, Devices and Applications II*, J. D. Gonglewski, M. T. Gruineisen, and M. K. Giles, eds., *Proc. SPIE* **5553**, pp. 1–16, 2004.
3. J. W. Evans, G. Sommargren, B. A. Macintosh, S. Severson, and D. Dillon, "Effect of wavefront error on 10^{-7} contrast measurements," *Optics Letters* **submitted**, 2005.
4. N. J. Kasdin, R. J. Vanderbei, D. N. Spergel, and M. G. Littman, "Extrasolar planet finding via optimal apodized-pupil and shaped-pupil coronagraphs," *Astrophysical Journal* **582**(2), pp. 1147–61.
5. J. W. Evans, K. Morzinski, L. Reza, S. Severson, L. Poyneer, B. Macintosh, D. Dillon, G. Sommargren, D. Palmer, D. Gavel, and S. Olivier, "Extreme adaptive optics testbed: High contrast measurements with a mems deformable mirror," in *Techniques and Instrumentation for Detection of Exoplanets II*, D. R. Coulter, ed., *Proc. SPIE* **5905**, pp. 303–310, 2005.
6. G. E. Sommargren, D. W. Phillion, M. A. Johnson, N. Q. Nguyen, A. Barty, F. J. Snell, D. R. Dillon, and L. S. Bradsher, "100-picometer interferometry for euvl," in *Emerging Lithographic Technologies VI*, R. L. Engelstad, ed., *Proc. SPIE* **4688**, pp. 316–328, 2002.
7. H. R. Shea, A. Gasparyan, C. D. White, R. B. Comizzoli, D. Abushch-Magder, and S. Arney, "Anodic oxidation and reliability of mems poly-silicon electrodes at high relative humidity and high voltages," in *MEMS Reliability for Critical Applications*, R. A. Lawton, ed., *Proc. SPIE* **4180**, pp. 117–122, 2000.